Origin of Kern's arc

Yoshihide Takano and Kuo-Nan Liou

With the aid of computer-simulated halo patterns, we show that Kern's arc, as seen on the latitude of the circumzenithal arc and on the other side of the zenith, is produced by double-plate ice crystals with a vertical principal axis. Light rays that contribute to Kern's arc are demonstrated by geometric ray tracing. We also discuss the condition under which an arc that is opposite a circumhorizontal arc can appear. © 1997 Optical Society of America

Key words: Meteorological optics, halo phenomena.

1. Introduction

Two kinds of Kern's arc have been observed. One is a complete white circle on the latitude of the circumzenithal arc.[1,2] The other is an arc located on the same latitude as the circumzenithal arc but on the opposite side of the zenith.[3–5] The former has been interpreted in terms of multiple scattering with the aid of ray-tracing simulations presented by Tränkle and Greenler[6] and Takano and Liou.[7] The origin of the latter is not yet known,[8–10] however. Here we investigate the cause of the latter Kern's arc by simulating a halo pattern with the Monte Carlo geometric ray-tracing technique that we developed recently.[11]

Approximately 90% of the observed ice crystals in cumulus clouds have developed a structure of double plates,[12] generally consisting of one column with a plate attached to each end.[13] To investigate the effect of this shape structure on light scattering, we used a combination of one column and two plates with different aspect ratios connected by their principal axes, as shown in Fig. 1, where l_1, l_2, and l_3 are the lengths of each crystal, and $2a_1$, $2a_2$, and $2a_3$ are the corresponding widths. For the identification of halo positions, a geometric ray-tracing program for reflections and/or refractions is sufficient. Because the procedure of geometric ray tracing for irregular crystals has been detailed in our recent paper,[11] here we present only a brief outline.

Let a bundle of parallel rays, which can be regarded as a flow of photons, be incident on a crystal from a certain direction. Consider a plane normal to this bundle of incident rays and the geometric shadow of the crystal projected onto this plane. The incident point of a photon in the projected area of the ice crystal is then determined by random numbers. A crystal plane containing three points can be expressed in Cartesian coordinates. The incident photons can then be traced geometrically with a hit-and-miss Monte Carlo method. Numbers of the scattered photons per unit solid angle are counted at each scattering direction. They are subsequently integrated with respect to the crystal azimuthal angle around the principal axis so that the normalized phase function can be computed. In the present analysis, the tip angle for the horizontally oriented plate crystals is assumed to be 0°.

2. Computational Results and Discussion

Figures 2(a) and 2(b) show a fish-eye view of the intensity pattern for the visible light scattered by double plates and single plates with a vertical principal axis. The assumed crystal geometry is illustrated in the upper part of each figure. For the demonstration of optical phenomena produced by the visible wavelength, it suffices to use the relative ice crystal lengths and widths in the discussion. Examples of these values are listed in Table 1 in conjunction with a number of graphic presentations. The equivalent single plate shown in Fig. 2(b) with an aspect ratio of $L/2a$ of 0.25/2 has the same projected area and an averaged aspect ratio as the double plate shown in Fig. 2(a). The small circles in Figs. 2(a) and 2(b) depict the apparent location of the Sun. For our analysis we used the solar zenith angle θ_0 of 72°. Figure 2 shows a number of well-known optical phenomena, including the circumzenithal arc, parhelic circle, and sun dogs. In the case of double plates, an additional arc is produced on the latitude but oppo-

The authors are with the Department of Meteorology, Center for Atmospheric and Remote Sounding Studies, University of Utah, 809 William C. Browning Building, Salt Lake City, Utah 84112.

Received 22 April 1996; revised manuscript received 8 July 1996.
0003-6935/97/153560-05$10.00/0

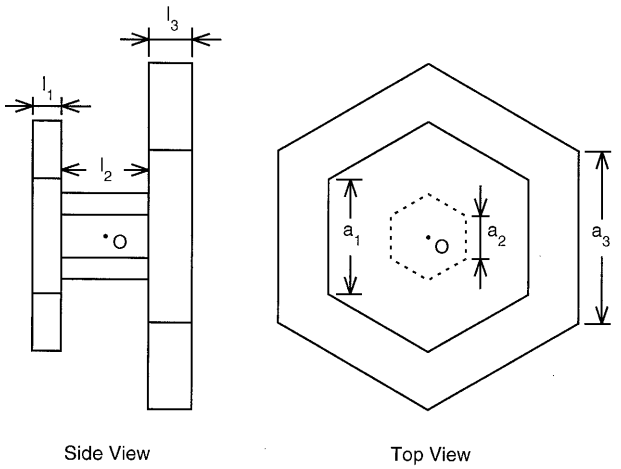

Fig. 1. Crystal geometry for a double plate.

site the zenith of the circumzenithal arc. This simulated arc, which is less than a semicircle in extent, resembles the observed Kern's arc reported in the literature.[3] In particular, we observed that the Kern's arc is fainter than the circumzenithal arc. This observation is consistent with the relatively weak intensity for Kern's arc displayed in Fig. 2(a).

In what follows, we explain the cause of Kern's arc using a geometric ray path, as shown in Fig. 3(a). A ray incident on the top of the upper plate is transmitted through the vertical prism plane and reaches the upper basal plane of the lower plate. It is then reflected totally off the vertical prism plane and emerges from the bottom of the lower plate. This

Table 1. Crystal Geometry in Arbitrary Units

Figure	$2a_1$	l_1	$2a_2$	l_2	$2a_3$	l_3
2(a)	1.2	0.1	0.2	0.2	1.6	0.2
3(b)	3.0	0.3	1.0	3.0	0.0	0.0
5(a)	1.2	0.2	0.2	0.2	0.8	0.1

ray path produces Kern's arc, which is a mirror image of the circumzenithal arc with respect to the zenith, as shown in Fig. 2(a). Even if the central hexagonal column were replaced by a frozen droplet, the ray path would remain unchanged and Kern's arc could still be simulated by geometric ray tracing.

The zenith angle θ^* of the circumzenithal arc is given by[7]

$$\theta^* = \pi/2 - \sin^{-1}(m_r^2 - \sin^2 \theta_0)^{1/2}, \qquad (1)$$

where $m_r(= 1.31)$ is the real part of the refractive index of ice. For the circumzenithal arc to occur without suffering total reflection, this angle θ^* must be larger than the critical angle $\sin^{-1}(m_r^2 - 1)^{1/2} \cong 58°$. According to Eq. (1), however, the angle θ^* is smaller than 32°. As a result, the ray displayed in Fig. 3(a) is always totally reflected off the prism plane after its reentry. Based on our simulations, Kern's arc occurs when the widths a_1 and a_3 of the double plate are varied simultaneously such that their difference is a constant value of 0.2, and, at the same time, the other lengths are unchanged. For example, the values of $(2a_1, 2a_3)$ can be (1.0, 1.4) or (1.4, 1.8). This arc can be enhanced in intensity if the length of the first ice crystal l_1 is doubled (see Table

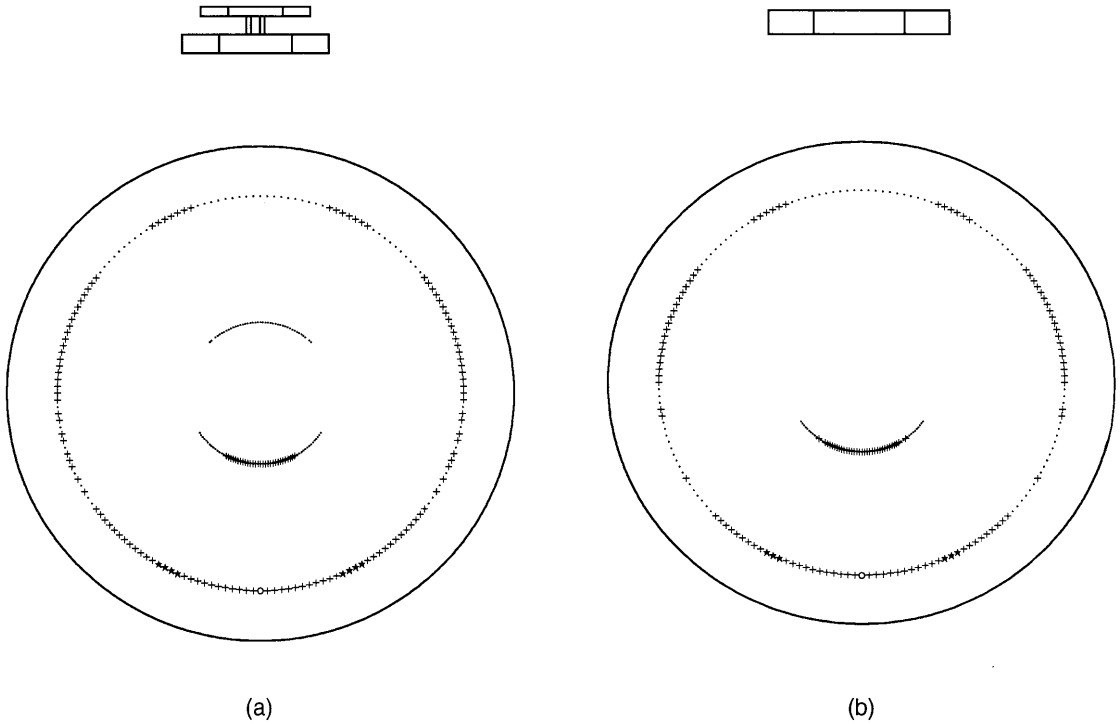

Fig. 2. Intensity distribution for the horizontally oriented (a) double plates and (b) single plates at 0.55-μm wavelength. The solar zenith angle θ_0 is 72°. The ★, +, and · are, respectively, 2, 1, and 0 in units of the integral part of a common logarithm of the phase function.

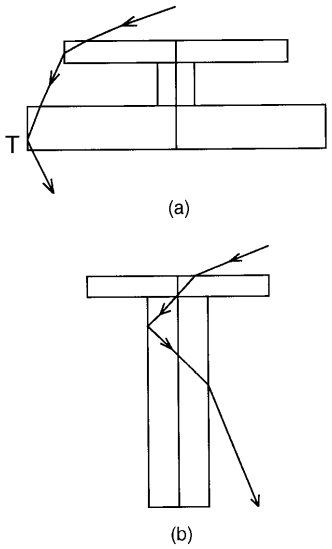

Fig. 3. (a) Geometric ray path that contributes to Kern's arc. *T* denotes the total reflection. (b) The ray path suggested by Humphreys that contributes to Kern's arc.

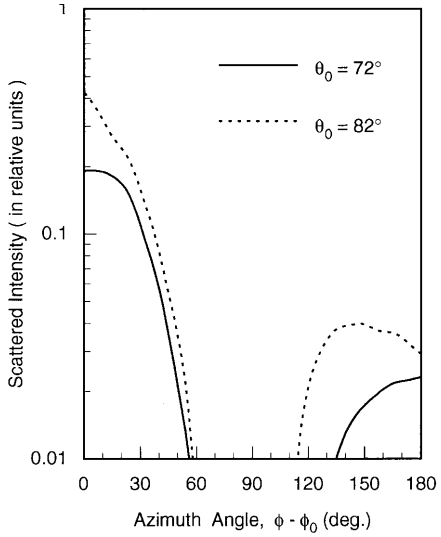

Fig. 4. Scattered intensity for the horizontally oriented double plates of the crystal geometry shown in Fig. 3(a) along the circumzenithal latitude for $\theta_0 = 72°$ and 82° at 0.55-μm wavelength.

1). We used $\theta_0 = 72°$ for the above analysis. If we increase this angle by approximately 10° (e.g., 82°), the arc will occur. However, it disappears if the solar zenith angle is decreased by approximately 10° (e.g., 62°), except when $2a_1$ has a value of 1.4. These simulated results are based on the tracing of the ray path as illustrated in Fig. 3(a).

Humphreys[14] suggested that the ray path displayed in Fig. 3(b) for the capped column can contribute to Kern's arc for a solar zenith angle of 68°. However, we were unable to simulate this arc using the capped-column model. In our simulation, the intensity distribution along the latitude circle of the circumzenithal arc, having a minimum at the azimuthal angle $\phi - \phi_0$ of 180°, is similar to that shown by Takano and Liou.[15] The internal reflection associated with the vertical prism plane in Fig. 3(b) does not undergo total reflection, resulting in a weaker (approximately 1 order of magnitude) scattered intensity around the azimuthal angle of 180° than the intensity shown in Fig. 2(a) that is produced by the geometry in Fig. 3(a).

Figure 4 shows the scattered intensities for horizontally oriented double plates along the circumzenithal latitude. The circumzenithal arc and Kern's arc occur at the azimuthal angles $\phi - \phi_0 < 60°$ and $\phi - \phi_0 > 110°$, respectively. Figure 4 shows that the circumzenithal arc produced by single plates is comparable with that produced by double plates. Usually, the circumzenithal arc in nature can be observed for an azimuthal angle as large as 60°. Thus, Kern's arc, as illustrated in Fig. 4, should also be observable in view of the computed intensity. The circumzenithal circle illustrated by Tränkle and Greenler,[6] based on multiple scattering computations, does not have a dip in the scattered intensity in the $60° < \phi - \phi_0 < 120°$ region as our results show. The simulated intensity patterns indicate that the preceding arcs are the production of a combination of two different optical phenomena that are related to two distinct physical mechanisms. This argument is reinforced by the fact that the circumzenithal circle is white as a result of multiple scattering, whereas Kern's arc is in color because of single scattering only.[9]

Figures 5(a) and 5(b) show the intensity patterns for light scattered by horizontally oriented double plates and single plates with an aspect ratio of 0.24/1.44 for $\theta_0 = 27°$. The double plates in Fig. 5(a) are assumed to fall with the smaller plate on the bottom. Note that the double plates displayed in Fig. 2(a) are assumed to fall with the smaller plate on the top. Because rimming can be observed on the inner side along the surface of the larger plate of a double-plate crystal, it would fall with the smaller plate on the bottom.[12] However, because of the tipping effect, both fall modes are possible. Although Iwai[16] found that double plates tend to fall with the smaller plates on the bottom, the other fall mode appears to be more likely if widths a_1 and a_3 of the two plates have similar values (see Figs. 2 and 5). The problem of the fall position of a double-plate crystal is still a subject of uncertainty.[17] Both configurations in Fig. 5 produce the parhelic circle and circumhorizontal arc. However, an additional faint arc occurs on the latitude of the circumhorizontal arc and on the opposite side of the zenith in the double-plate configuration depicted in Fig. 5(a). This arc is referred to as the anticircumhorizontal arc. A ray path that contributes to it is shown in Fig. 6. The ray incident on the vertical prism plane of the upper plate that is transmitted and reenters into the lower plate may or may not pass through the column between. This ray is then reflected off the prism plane and emerges from the bottom of the lower plate. In contrast to Kern's arc, the intensity of the anticircumhorizontal arc is weak, and it appears only for the crystal geometry

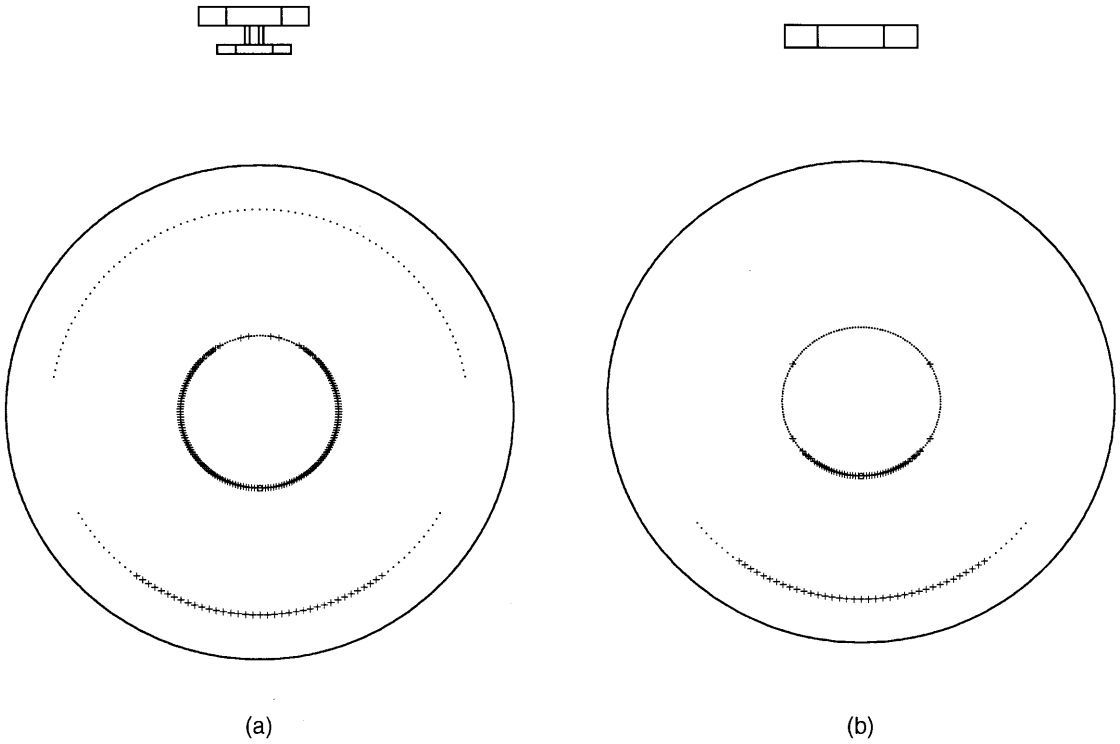

Fig. 5. Intensity distribution for the horizontally oriented (a) double plates and (b) single plates at 0.55-μm wavelength. The solar zenith angle θ_0 is 27°. The symbols + and · are the same as those in Fig. 2.

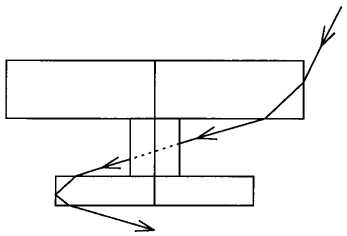

Fig. 6. Ray path that contributes to the anticircumhorizontal arc defined in this paper.

defined in Fig. 6 with a solar zenith angle of 27°. It vanishes when the crystal geometry and solar zenith angle vary slightly. The weak intensity in this case results because of the absence of total reflection at the prism plane after reentry (see Fig. 6). The simulated anticircumhorizontal arc presented here appears to be quite unique. To the best of our knowledge, no record of such an arc has been reported in the literature.

3. Concluding Remarks

The origin of Kern's arc has been examined by using a Monte Carlo geometric ray-tracing method. The simulated Kern's arc, which was produced by the ray undergoing total internal reflection as shown in Fig. 3(a), can be observed because of its appreciable intensity and the abundant existence of double plates in cumulus clouds. The arc that has been reported by a number of observers[3,4,9] is probably Kern's arc produced by the horizontally oriented double plates. We have determined that the ray path suggested by Humphreys[14] cannot be the origin of Kern's arc. We also note that neither the horizontally oriented triangular plates[9] nor the horizontally oriented hexagonal plates[8,10] can produce Kern's arc because of the insufficient scattered intensities around the azimuthal angle of 180°.

This research was supported by the National Science Foundation under grant ATM93-15251.

References

1. C. S. Ling, "Complex solar halo observed at Ellendale, N. Dak.," Mon. Weather Rev. **50,** 132–133 (1922).
2. E. A. Ripley and B. Saugier, "Photometeors at Saskatoon on 3 December 1970," Weather **26,** 150–157 (1971).
3. Anonymous, "Halos of March 1–4 1906," Mon. Weather Rev. **34,** 123–124 (1906).
4. L. Besson, "The halos of November 1 and 2, 1913," Mon. Weather Rev. **42,** 431–446 (1914).
5. R. A. R. Tricker, *Ice Crystal Haloes* (Optical Society of America, Washington, D.C., 1979), Chaps. 1 and 7.
6. E. Tränkle and R. G. Greenler, "Multiple-scattering effects in halo phenomena," J. Opt. Soc. Am. A **4,** 591–599 (1987).
7. Y. Takano and K. N. Liou, "Halo phenomena modified by multiple scattering," J. Opt. Soc. Am. A **7,** 885–889 (1990).
8. R. G. Greenler, *Rainbow, Halos, and Glories* (Cambridge U. Press, New York, 1980), Chap. 3, p. 96.
9. W. Tape, *Atmospheric Halos* (American Geophysical Union, Washington, D.C., 1994), Chap. 11, pp. 101–104.
10. D. K. Lynch and W. Livingston, *Color and Light in Nature* (Cambridge U. Press, New York, 1995), Chap. 5, p. 166.
11. Y. Takano and K. N. Liou, "Radiative transfer in cirrus clouds. Part III: Light scattering by irregular ice crystals," J. Atmos. Sci. **52,** 818–837 (1995).

12. R. T. Bruintjes, A. J. Heymsfield, and T. W. Krauss, "An examination of double-plate ice crystal and the initiation of precipitation in continental cumulus clouds," J. Atmos. Sci. **44,** 1331–1349 (1987).
13. A. J. Heymsfield, "Laboratory and field observations of the growth of columnar and plate crystals from frozen droplets," J. Atmos. Sci. **30,** 1650–1656 (1973).
14. W. J. Humphreys, *Physics of the Air* (McGraw-Hill, New York, 1940), Chap. 4, pp. 513–514.
15. Y. Takano and K. N. Liou, "Solar radiative transfer in cirrus clouds. Part I: Single-scattering and optical properties of hexagonal ice crystals," J. Atmos. Sci. **46,** 3–19 (1989).
16. K. Iwai, "Three-dimensional structure of plate-like snow crystals," J. Meteorol. Soc. Jpn. **61,** 746–755 (1983).
17. N. Fukuta, M. W. Kowa, and N. H. Gong, "Determination of ice crystal growth parameters in a new supercooled cloud tunnel," in *Proceedings of the Conference on Cloud Physics* (American Meteorological Society, Dallas, Tex., 1982), pp. 325–328.